INTERNATIONAL JOURNAL FOR NUMERICAL METHODS IN ENGINEERING
Int. J. Numer. Meth. Engng 2006; **66**:461–484
Published online 12 December 2005 in Wiley InterScience (www.interscience.wiley.com). DOI: 10.1002/nme.1560

Topology optimization of creeping fluid flows using a Darcy–Stokes finite element

James K. Guest*,† and Jean H. Prévost‡

Department of Civil and Environmental Engineering, Princeton University, Princeton, NJ 08544, U.S.A.

SUMMARY

A new methodology is proposed for the topology optimization of fluid in Stokes flow. The binary design variable and no-slip condition along the solid–fluid interface are regularized to allow for the use of continuous mathematical programming techniques. The regularization is achieved by treating the solid phase of the topology as a porous medium with flow governed by Darcy's law. Fluid flow throughout the design domain is then expressed as a single system of equations created by combining and scaling the Stokes and Darcy equations. The mixed formulation of the new Darcy–Stokes system is solved numerically using existing stabilized finite element methods for the individual flow problems. Convergence to the no-slip condition is demonstrated by assigning a low permeability to solid phase and results suggest that auxiliary boundary conditions along the solid–fluid interface are not needed. The optimization objective considered is to minimize dissipated power and the technique is used to solve examples previously examined in literature. The advantages of the Darcy–Stokes approach include that it uses existing stabilization techniques to solve the finite element problem, it produces 0–1 (void–solid) topologies (i.e. there are no regions of artificial material), and that it can potentially be used to optimize the layout of a microscopically porous material. Copyright © 2005 John Wiley & Sons, Ltd.

KEY WORDS: topology optimization; stabilized finite element methods; porous media; coupled flow; Darcy's law; Stokes equations

1. INTRODUCTION

This paper presents a new technique for the topology optimization of creeping fluid flows. The material phase in the design problem is treated as a porous medium with Darcy's law

*Correspondence to: James K. Guest, Department of Civil Engineering, Johns Hopkins University, 3400 N. Charles St., Baltimore, MD 21218, U.S.A.
†E-mail: jkguest@jhu.edu, jkguest@princeton.edu
‡E-mail: prevost@princeton.edu

Contract/grant sponsor: NASA University Research, Engineering and Technology Institute on Bio Inspired Materials (BIMat); contract/grant number: NCC-1-02037

Received 13 May 2005
Revised 31 August 2005
Accepted 26 September 2005

governing fluid velocities. The governing equations for flow throughout the domain are then expressed as a single system of equations, allowing for the use of continuous mathematical programming techniques.

The application of optimization methods to viscous fluid flow problems has been an active area of research for several decades. There is a wealth of literature on optimal control of flows through suction and injection of fluid along domain boundaries (see, e.g. References [1–3]). In the context of design, shape optimization has been applied to (for example) the design of minimum drag bodies [4–7], diffusers [8, 9], valves [10], and airfoils [11, 12]. Generally, the stated objective is to minimize drag, minimize the rate at which energy is dissipated, and/or minimize pressure drop across the domain. Only recently has topology optimization been used to design fluid transport and minimum drag devices. Shape optimization is limited to determining the shape of an existing boundary of a fluid body (domain) whereas topology optimization can be used to design features within the domain, allowing new boundaries to be introduced into the design.

Topology optimization of structures is a well-documented field. The goal is to determine the layout of material in a given design domain Ω that minimizes the objective function for a given set of loads and boundary conditions. The layout of material within Ω is expressed by the discrete valued material distribution function $\rho(\mathbf{x})$, where $\mathbf{x}$ is the location inside Ω. For two-phase solid–void problems, $\rho(\mathbf{x}) = 1$ when material is present, and 0 otherwise. To solve the optimization problem, the design domain is usually discretized using finite elements. The material distribution function is defined as constant inside each elemental domain and is denoted as ρ^e, the element volume fraction, or relative density. Each element is thus considered a solid element (with material) when $\rho^e = 1$ and a void element (without material) when $\rho^e = 0$, with the structure defined by the connectivity of the solid elements. The reader is referred to References [13, 14] for an overview.

Solving for the optimal discrete valued variables ρ^e used to define topology requires discrete optimization algorithms. Integer programming techniques such as branch-and-bound, however, are generally computationally prohibitive, especially for large-scale optimization problems. The most common procedure for circumventing this issue is to relax the binary constraint and allow element volume fractions to achieve intermediate values, values between 0 and 1. Although now permitted, intermediate volume fractions represent fictitious material and are thus penalized to drive the solution to a 0–1 topology.

Only recently has topology optimization been applied to fluids. Borrvall and Petersson [15] implemented the relaxed material distribution approach to minimize the power dissipated in creeping flows of Newtonian fluids, i.e. fluids in Stokes flow. Considering only an impermeable solid phase, they approximate the no-slip condition along the solid–fluid interface by using a generalized Stokes problem to govern fluid flow throughout the domain. The generalized problem is derived from a plane flow assumption (Coulette flow): three-dimensional flow is reduced to a two-dimensional problem by assuming that the fluid flows between plates separated by a distance of $2(1 - \rho^e)$ in the third dimension. Large elemental volume fractions then represent narrow channel flow, thereby decreasing fluid velocities in these elements. This assumption is reflected in the finite element formulation by introducing a damping term, designated as an 'inverse permeability', to the Stokes viscosity stiffness matrix. The damping term is related to the element volume fraction ρ^e through a convex parameterized interpolation function with the following properties: (i) the damping term is close to zero for void elements, meaning Stokes flow dominates while (ii) the damping term is large and dominates for solid

elements, thereby greatly reducing the corresponding nodal velocities. Although the physical representation of Coulette flow is lost for three-dimensional flow, the numerical technique is still applicable.

The goal of this work is to improve upon the relaxed Stokes flow formulation proposed in Reference [15]. Rather than use a numerical damping term derived from a seemingly unrelated flow condition, we treat the material phase as a porous medium where fluid flow is governed by Darcy's law. For impermeable solid material, the no-slip condition is simulated by using a small value for the material permeability to obtain negligible fluid velocities at the nodes of solid elements. The flow regularization can be expressed as a system of equations by combining and scaling the Stokes and Darcy equations so that Stokes flow governs in void elements and Darcy flow governs in solid elements. The combination resembles Brinkman's equation for flow through multiple scale porous media and will be referred to as the Darcy–Stokes equations. These equations are solved using a combination of established stabilized finite element formulations developed for the individual flow problems. Preliminary results suggest that this technique is capable of accurately modelling flow in both domains and that the solid–fluid interface does not require special treatment such as auxiliary meshes, additional boundary conditions, or interface stabilization schemes.

Although of similar structure to the generalized Stokes problem of Reference [15], the Darcy–Stokes formulation is distinctly different. First, the Darcy–Stokes flow problem can be conveniently solved using existing stabilized finite elements with equal-order interpolations for the velocity and pressure fields. The approach in Reference [15], on the other hand, uses different size meshes to solve for the velocity and pressure variables. Second, both formulations as derived are capable of simulating the no-slip condition. The Darcy–Stokes formulation, however, could also potentially be used to optimize the layout of a microscopically porous material, such as in the design of filters. This opens the door for designing on two length scales: optimizing the macroscopic layout of a permeable material as well as the porous microstructure of that material.

The remainder of the paper is as follows. Section 2 discusses the Stokes flow equations and topology optimization problem for fluids in Stokes flow. Section 3 introduces the Darcy flow regularization and the corresponding optimization problem. Section 4 presents the optimization algorithm and Section 5 contains results for example problems. Concluding remarks are given in Section 6.

2. THE STOKES FLOW OPTIMIZATION PROBLEM

The topology optimization problem is confined to a given design domain Ω that is composed of solid material and voids through which a viscous fluid flows. The goal is to find the layout of voids (fluid) of volume V_f that minimizes a power function $f(\rho, \mathbf{u})$ for a given set of boundary conditions, where $\mathbf{u}$ are the fluid velocities. The fluid flow is assumed to be incompressible, steady, and slow so that Stokes equations govern. For simplicity and consistency with Reference [15], the presented problem is formulated for an impermeable solid material so that the no-slip condition along the solid–fluid interface is enforced. Necessary changes for optimizing the layout of a permeable material are noted where appropriate.

2.1. Problem formulation

The Stokes flow problem is to find the velocity–pressure pair that satisfies the following conditions:

$$\begin{aligned} \nabla\cdot\boldsymbol{\sigma}+\rho_{\mathrm{f}}\mathbf{b}&=\mathbf{0}\\ \nabla\cdot\mathbf{u}&=0\\ \mathbf{u}(\mathbf{x})&=\mathbf{g}(\mathbf{x})\quad\forall\mathbf{x}\in\Gamma_g\\ \boldsymbol{\sigma}(\mathbf{x})\cdot\mathbf{n}(\mathbf{x})&=\mathbf{h}(\mathbf{x})\quad\forall\mathbf{x}\in\Gamma_h \end{aligned} \tag{1}$$

where ρ_{f} is the fluid mass density, $\mathbf{b}$ is the body force vector per unit mass, $\mathbf{n}(\mathbf{x})$ is the unit normal to the boundary at location $\mathbf{x}$, $\mathbf{g}$ provides velocity boundary conditions acting on the boundary Γ_g, and $\mathbf{h}$ provides the traction boundary conditions acting on the boundary Γ_h. The Cauchy stress $\boldsymbol{\sigma}$ is computed by

$$\boldsymbol{\sigma}=2\mu\mathbf{D}-p\mathbf{I} \tag{2}$$

where μ is the dynamic viscosity, p is the pressure, $\mathbf{I}$ is the identity tensor, and $\mathbf{D}$ is the symmetrical part of the velocity gradient:

$$\mathbf{D}=\tfrac{1}{2}(\nabla\mathbf{u}+(\nabla\mathbf{u})^{\mathrm{T}}) \tag{3}$$

Note that for the common case where Γ_h is empty, the following condition holds:

$$\int_{\Gamma}\mathbf{g}\cdot\mathbf{n}\,\mathrm{d}\Gamma=0 \tag{4}$$

Substituting the definition of the fluid stress and expanding, the Stokes flow equations can be expressed as

$$\begin{aligned} \mu\nabla^2\mathbf{u}-\nabla p&=-\rho_{\mathrm{f}}\mathbf{b}\\ \nabla\cdot\mathbf{u}&=0 \end{aligned} \tag{5}$$

The general material distribution optimization problem governed by Stokes flow is thus stated as

$$\begin{aligned} &\min_{\rho,\,\mathbf{u},\,p} f(\rho,\mathbf{u})\\ &\text{subject to:}\quad \mu\nabla^2\mathbf{u}(\mathbf{x})-\nabla p(\mathbf{x})=-\rho_{\mathrm{f}}\mathbf{b}(\mathbf{x})\\ &\qquad\qquad \nabla\cdot\mathbf{u}(\mathbf{x})=0\\ &\qquad\qquad \mathbf{u}(\mathbf{x})=\mathbf{g}(\mathbf{x})\quad\forall\mathbf{x}\in\Gamma_g\\ &\qquad\qquad \mathbf{u}(\mathbf{x})=\mathbf{0}\quad\forall\mathbf{x}\in\Gamma_{\mathrm{s}}\\ &\int_{\Omega}(1-\rho(\mathbf{x}))\,\mathrm{d}\Omega\leqslant V_{\mathrm{f}}\\ &\qquad\qquad \rho(\mathbf{x})=\{0,1\}\quad\forall\mathbf{x}\in\Omega \end{aligned} \tag{6}$$

where

$$\mathbf{x} \in \begin{cases} \Omega_s & \text{if } \rho(\mathbf{x}) = 1 \\ \Omega_f & \text{if } \rho(\mathbf{x}) = 0 \end{cases}$$

and $f(\rho, \mathbf{u})$ is the power function to be minimized, ρ is the previously discussed material distribution function, Ω_s and Ω_f are the regions of solid material and fluid ($\Omega = \Omega_s \cup \Omega_f$), respectively, and the fourth constraint represents the no-slip, or adherence, condition, where Γ_s is the boundary of Ω_s. Note that Stokes equations and the no-slip condition govern flow in Ω_f and on Γ_s, respectively. The locations of these regions are dictated by topology, and thus change as the design variable ρ changes.

2.2. The discretized design optimization problem

The Stokes equations can be solved numerically using finite elements. In the mixed formulation where velocity and pressure are the variables, a stability condition regarding the velocity and pressure spaces must be satisfied for the problem to be solved. Known as the Babuska–Brezzi condition [16, 17], this restriction can be circumvented by using a Petrov–Galerkin formulation proposed by Hughes *et al.* [18]. This technique allows for the use of equal-order interpolations for both the velocity and pressure, making it particularly attractive. The matrix form of the stabilized Stokes flow problem is given as

$$\begin{bmatrix} \mathbf{K}_s & -\mathbf{G}_s \\ \mathbf{L}_s + \mathbf{G}_s^T & \mathbf{M}_s \end{bmatrix} \begin{bmatrix} \mathbf{u} \\ \mathbf{p} \end{bmatrix} = \begin{bmatrix} \mathbf{f}_s \\ \mathbf{h}_s \end{bmatrix} \tag{7}$$

where $\mathbf{K}_s$ is the viscosity stiffness matrix, $\mathbf{G}_s$ is the gradient matrix, $\mathbf{G}_s^T$ is the divergence matrix, $\mathbf{L}_s$ is the consistency matrix, and $\mathbf{M}_s$ is the stabilization matrix. The subscript 's' has been added to denote Stokes flow. The global matrices on the left-hand side are assembled from the element matrices $\mathbf{k}_s^e$, $\mathbf{G}_s^e$, $\mathbf{L}_s^e$, $\mathbf{G}_s^{e^T}$, and $\mathbf{M}_s^e$ in the usual manner. The consistency and stabilization matrices do not appear in the classical Galerkin formulation and result from perturbation of the weighting functions as described in Reference [18]. Note that $\mathbf{u}$ and $\mathbf{p}$ are now only the unknown nodal velocities and pressures, respectively, and $\mathbf{f}_s$ and $\mathbf{h}_s$ are the nodal forces resulting from body forces and boundary conditions.

A common approach used in the topology optimization of structures for minimum compliance is to express the equilibrium constraint as a minimum potential energy problem in the objective function. Similarly, as demonstrated in Reference [15], it is useful to reformulate the Stokes equations constraint as a minimum potential power problem. The total potential power $\Theta(\mathbf{u})$ of a fluid is defined as

$$\Theta(\mathbf{u}) = \tfrac{1}{2}\, \tilde{\mathbf{u}}^T \tilde{\mathbf{K}}_s \tilde{\mathbf{u}} - \rho_f (\mathbf{b}_u)^T \mathbf{u} \tag{8}$$

where $\rho_f \mathbf{b}_u$ are the nodal body forces corresponding to the unknown velocities, $\tilde{\mathbf{K}}_s$ is the viscosity stiffness matrix for all velocity degrees of freedom (unknown and prescribed), and $\tilde{\mathbf{u}}$ is the complete velocity vector, i.e.

$$\tilde{\mathbf{u}} = \begin{bmatrix} \mathbf{u} \\ \mathbf{g} \end{bmatrix} \tag{9}$$

The velocities that solve Stokes equations can be found by minimizing the total potential power $\Theta(\mathbf{u})$ subject to the incompressibility condition. Define the subset U_{div} of admissible velocities U as

$$U_{\text{div}} = \{\mathbf{v} \in U \mid \nabla \cdot \mathbf{v} = 0\} \tag{10}$$

The minimum potential power $\Phi(\mathbf{u})$ is then defined as

$$\Phi(\mathbf{u}) = \min_{\mathbf{v} \in U_{\text{div}}} \Theta(\mathbf{v}) \tag{11}$$

The optimal velocities $\mathbf{u}$ of this problem are the velocities in the solution to (7). This can be seen by relaxing the divergence condition and forming the Lagrangian function. The first-order conditions for optimality yield a system of equations that is equivalent to Stokes equations when the Lagrange multiplier for the incompressibility constraint is interpreted as pressure.

The minimum total potential power Φ is chosen to be the objective function for the design optimization problem. To minimize Φ is to minimize the total dissipated power while maximizing velocities at locations of the applied (body) forces. Minimizing dissipated power is equivalent to minimizing drag or minimizing average pressure drop across the domain when prescribed velocities are uniform and normal to the boundary [15]. The objective is then to find the layout of voids (fluid) of volume V_{f} in the domain Ω that minimizes the minimum total potential power of the fluid for a given set of boundary conditions. The topology is defined by elementwise volume fractions ρ^e as in traditional structural optimization.

The binary discretized minimum potential power design problem is stated as

$$\begin{aligned} &\min_{\rho^e} \ \Phi(\rho^e, \mathbf{u}) \\ &\text{subject to:} \quad \sum_{e \in \Omega} (1 - \rho^e) v^e \leqslant V_{\text{f}} \\ &\qquad\qquad \mathbf{u}^e = \mathbf{0} \quad \text{if} \ \ \rho^e = 1 \\ &\qquad\qquad \rho^e = \{0, 1\} \quad \forall e \end{aligned} \tag{12}$$

where

$$\rho^e(\mathbf{x}) = \begin{cases} 1 & \text{if } \mathbf{x} \in \text{solid element} \\ 0 & \text{if } \mathbf{x} \in \text{void element} \end{cases}$$

and $\mathbf{u}^e$ are the nodal velocities for element e. Note that the second constraint represents the adherence condition as a function of topology.

2.3. Relaxing the binary constraint

This problem is extraordinarily difficult to solve as it is a binary moving-boundary optimization problem. Solving it would require discrete optimization algorithms and entail updating the nodal boundary conditions representing the no-slip condition at every design iteration. Therefore, the binary constraint is relaxed to allow intermediate volume fractions and the use of continuous

mathematical programming techniques. Accordingly, the explicit adherence condition must be regularized.

To recover the adherence condition and steer the solution to a 0–1 topology, stiffness matrices of non-void elements are augmented to decrease the corresponding nodal velocities. Borrvall and Petersson [15] make a plane flow assumption to derive a generalized Stokes flow problem of the following form:

$$\begin{gathered}(\mu\nabla^2 - \alpha(\rho))\mathbf{u} - \nabla p = -\rho_f \mathbf{b} \\ \nabla \cdot \mathbf{u} = 0\end{gathered} \tag{13}$$

where $\alpha(\rho)$ can be called an inverse permeability function and is used to slow velocities in solid elements. In its derived form, α is expressed as $\alpha(\rho) = 2.5\mu/\rho^2$ which has been adjusted from Reference [15] to match our definition for solid material present ($\rho = 1$). For numerical reasons, however, Borrvall and Petersson implement a convex non-linear parameterized function to damp velocities:

$$\alpha(\rho) = \bar{\alpha} + (\underline{\alpha} - \bar{\alpha})(1 - \rho)\frac{1+q}{1-\rho+q} \tag{14}$$

where q is a parameter to control the degree of penalization and $\bar{\alpha}$ and $\underline{\alpha}$ are the magnitudes of alpha for a solid and void element, respectively. When substituting (14) into (13), the Stokes flow term dominates for void elements and the damping term dominates for solid elements. Note, however, that in this numerical representation the damping function is never zero, and therefore numerical damping, although small (e.g. $\underline{\alpha} = 2.5\mu/100^2$), is present in void elements.

We propose regularizing the solid–fluid interface by treating the material phase as a porous medium where fluid flow is governed by Darcy's law. To simulate the no-slip condition, a small non-zero number is used for the material permeability thereby yielding minimal fluid velocities at the nodes of solid elements. We believe this approach to be a more natural representation of flow during the optimization iterations when intermediate volume fractions exist. It also offers the potential to optimize the layout of a microscopically porous material. When the solid phase is permeable, fluid flow through solid elements would be governed by Darcy's law, while Stokes flow would still govern the flow through void elements. For example, this would be the conditions for the design of a filter.

3. THE DARCY FLOW REGULARIZATION

3.1. Darcy's law

Darcy's law for viscous flow with conservation of mass is given by

$$\begin{gathered}\mathbf{u} = -\frac{\kappa}{\mu}(\nabla p - \rho_f \mathbf{b}) \\ \nabla \cdot \mathbf{u} = 0 \\ \mathbf{u} \cdot \mathbf{n} = \psi \quad \text{on } \Gamma\end{gathered} \tag{15}$$

where κ is the permeability, ψ is the normal component of velocity on the boundary Γ, and $\mathbf{n}$ is the unit normal vector to the boundary.

As fluid velocity in Darcy's law is proportional to material permeability κ, the adherence can be recovered by using material with low permeability to represent solid elements.

For consistency with the Stokes formulation, the Darcy flow equations are solved using mixed finite element methods with velocity and pressure variables. The Babuska–Brezzi condition is circumvented via a stabilization proposed by Masud and Hughes [19]. This approach is particularly attractive in that it does not require mesh-dependent parameters and uses equal-order interpolations for the velocity and pressure fields. The stabilized matrix equation for Darcy flow is stated as

$$\begin{bmatrix} \mathbf{K}_\mathrm{d} & -\mathbf{G}_\mathrm{d} \\ \mathbf{G}_\mathrm{d}^\mathrm{T} & \mathbf{M}_\mathrm{d} \end{bmatrix} \begin{bmatrix} \mathbf{u} \\ \mathbf{p} \end{bmatrix} = \begin{bmatrix} \mathbf{f}_\mathrm{d} \\ \mathbf{h}_\mathrm{d} \end{bmatrix} \tag{16}$$

where $\mathbf{K}_\mathrm{d}$ is the viscosity stiffness matrix, $\mathbf{G}_\mathrm{d}$ is the modified gradient matrix, $\mathbf{G}_\mathrm{d}^\mathrm{T}$ is the modified divergence matrix, and $\mathbf{M}_\mathrm{d}$ is the stabilization matrix. The subscript 'd' has simply been added to indicate the tensors specific to Darcy flow. The element matrices $\mathbf{k}_\mathrm{d}^e$, $\mathbf{G}_\mathrm{d}^e$, $\mathbf{G}_\mathrm{d}^{e^\mathrm{T}}$, and $\mathbf{M}_\mathrm{d}^e$ are computed as described in Reference [19] and are assembled in the usual manner to form the global matrices on the left-hand side. Note that $\mathbf{u}$ and $\mathbf{p}$ are again the unknown nodal velocities and pressures, respectively, and $\mathbf{f}_\mathrm{d}$ and $\mathbf{h}_\mathrm{d}$ are the nodal forces.

3.2. The Darcy–Stokes equations

The combined problem is formulated so that fluid flow is governed by Stokes equations in void elements and Darcy's law in solid elements; i.e. so that the field equations take the following form:

$$\begin{aligned} \left((1-\rho(\mathbf{x}))\mu\nabla^2-\rho(\mathbf{x})\,\frac{\mu}{\kappa}\,\mathbf{I}\right)\mathbf{u}-\nabla p &= -\rho_\mathrm{f}\mathbf{b} \\ \nabla\cdot\mathbf{u} &= 0 \end{aligned} \tag{17}$$

Numerical modelling of fluids in Stokes flow and Darcy flow is well established. However, a less studied topic is the modelling of coupled flow where fluid in Stokes flow borders and interacts with a porous medium, such as in filters and the interaction of surface and groundwater flow. The coupled flow problem is difficult to solve because the differential operators in the Stokes and Darcy equations are of different orders. This leads to challenges in determining approximating function spaces that yield unified numerical stability of both flow models [20, 21]. Several approaches have been proposed to circumvent this difficulty along the interface of the Stokes flow and Darcy flow regions. The Brinkman equation for flow through multiple scale porous media includes a second-order velocity term, providing continuity of the velocity and pressure fields across the interface. It resembles Equation (17) but includes an effective viscosity term controlled by problem geometry that is meant to resolve the shear-rate discontinuity at the interface [22, 23]. Beavers and Joseph implemented slip-wall boundary conditions along the interface that rely on determination of a slip-wall coefficient based on physical parameters [24, 25]. Other approaches include an edge stabilization technique proposed by Burman and Hansbo [21] that uses unequal-order approximation functions for the velocity and pressure fields and splits the viscous stress on the interface into normal and tangential components. Nassehi *et al.* [26] also use unequal-order approximation functions and propose a linking scheme that links elements along the interface by modifying the global stiffness assembly routine.

Although these techniques have been reported to produce good results for select problems, they require special treatment of the interface between regions of Stokes flow and Darcy flow. This would essentially negate the regularization, and therefore prohibit the use of continuous mathematical programming techniques. We have found it sufficient to solve the combined flow problem (17) by simply using the Stokes and Darcy stabilized finite element formulations previously discussed without special treatment of the interface.

The matrix formulation of the combined stabilized Stokes and stabilized Darcy flow is given by

$$\begin{bmatrix} \mathbf{K}_{\mathrm{ds}}(\rho^e) & -\mathbf{G}_{\mathrm{ds}}(\rho^e) \\ \mathbf{G}_{\mathrm{ds}}^{\mathrm{T}}(\rho^e) & \mathbf{M}_{\mathrm{ds}}(\rho^e) \end{bmatrix} \begin{bmatrix} \mathbf{u} \\ \mathbf{p} \end{bmatrix} = \begin{bmatrix} \mathbf{f}_{\mathrm{ds}}(\rho^e) \\ \mathbf{h}_{\mathrm{ds}}(\rho^e) \end{bmatrix} \tag{18}$$

where the combined Darcy–Stokes viscosity matrix $\mathbf{K}_{\mathrm{ds}}$, gradient matrix $\mathbf{G}_{\mathrm{ds}}$, divergence matrix $\mathbf{G}_{\mathrm{ds}}^{\mathrm{T}}$, and stabilization matrix $\mathbf{M}_{\mathrm{ds}}$ are assembled in the following manner:

$$\begin{aligned} \mathbf{K}_{\mathrm{ds}}(\rho^e) &= \mathop{\mathrm{A}}_{e} \mathbf{k}_{\mathrm{ds}}^e(\rho^e) = \mathop{\mathrm{A}}_{e}((1-\rho^e)\mathbf{k}_{\mathrm{s}}^e + \rho^e \mathbf{k}_{\mathrm{d}}^e) \\ \mathbf{G}_{\mathrm{ds}}(\rho^e) &= \mathop{\mathrm{A}}_{e}((1-\rho^e)\mathbf{G}_{\mathrm{s}}^e + \rho^e \mathbf{G}_{\mathrm{d}}^e) \\ \mathbf{G}_{\mathrm{ds}}^{\mathrm{T}}(\rho^e) &= \mathop{\mathrm{A}}_{e}((1-\rho^e)(\mathbf{L}_{\mathrm{s}}^e + \mathbf{G}_{\mathrm{s}}^{e^{\mathrm{T}}}) + \rho^e \mathbf{G}_{\mathrm{d}}^{e^{\mathrm{T}}}) \\ \mathbf{M}_{\mathrm{ds}}(\rho^e) &= \mathop{\mathrm{A}}_{e}((1-\rho^e)\mathbf{M}_{\mathrm{s}}^e + \rho^e \mathbf{M}_{\mathrm{d}}^e) \end{aligned} \tag{19}$$

where $\mathop{\mathrm{A}}_{e}$ is the standard finite element assembly routine. In other words, void elements have Stokes stiffness, solid elements have Darcy stiffness, and elements with intermediate volume fractions have a linearly weighted combination of Stokes and Darcy stiffness.

The nodal forces on the right-hand side are computed in a similar manner. For example, $\mathbf{f}_{\mathrm{ds}}$ is computed via

$$\mathbf{f}_{\mathrm{ds}}(\rho^e) = \rho_{\mathrm{f}} \mathbf{b}_{\mathrm{u}} - \mathop{\mathrm{A}}_{e}(\mathbf{k}_{\mathrm{ds}}^e(\rho^e)\mathbf{g}^e) \tag{20}$$

where $\mathbf{g}^e$ are the prescribed nodal velocity boundary conditions for element e, and the Darcy–Stokes element stiffness matrix $\mathbf{k}_{\mathrm{ds}}^e(\rho^e)$ is defined in Equation (19).

Note that the formulation given by (19) allows ρ^e to obtain the bounds of zero and one without losing positive-definiteness of the global stiffness matrix. This is unlike topology optimization of structures that requires a small non-zero minimum allowable volume fraction to maintain positive-definiteness.

3.3. Convergence to the no-slip condition

To demonstrate the capability of the Darcy regularization in replicating the no-slip condition, flow through the channel shown in Figure 1 was modelled using (i) Stokes finite elements with the no-slip condition implemented through boundary conditions and (ii) Darcy–Stokes finite elements. The inlet and outlet flows are prescribed to be fully developed laminar flow with unit maximum velocity between parallel plates. That is, they are prescribed normal to the boundary and parabolic, computed via the expression: $g(y) = 1-(2y/l)^2$, where y is the vertical distance

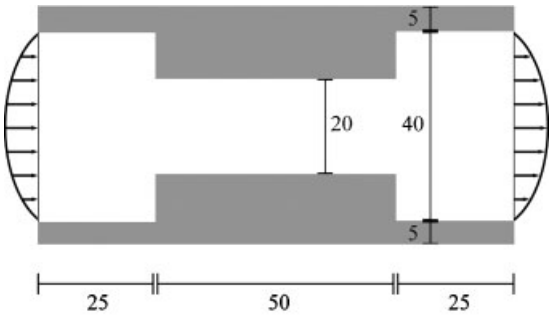

Figure 1. The channel topology for testing the Darcy–Stokes model.

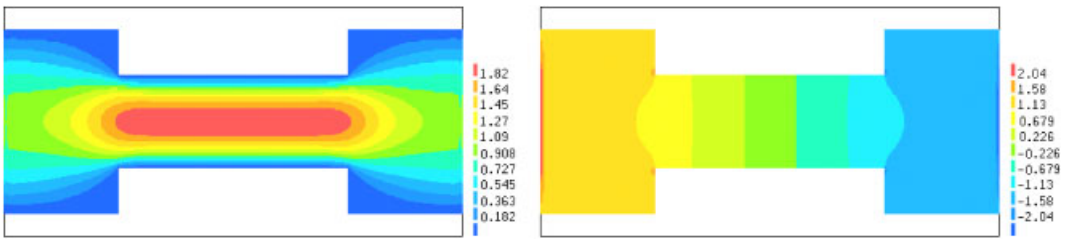

Figure 2. The velocity magnitude (left) and pressure (right) contours for the channel flow problem. Obtained using Stokes flow finite elements with no-slip boundary conditions along the solid–fluid interface. The maximum computed velocity is 2.00 occurring in the narrow channel.

from centre of domain ($y \in [-l/2, l/2]$) and l is the length of the flow boundary ($l = 40$). Pressure is prescribed to be zero at the centre of the domain to improve performance of iterative solvers. Units have been neglected for simplicity and all computations use 4-node quadrilateral elements.

Figure 2 displays the 'true' velocity magnitude and pressure contour plots obtained by meshing only the fluid domain with 12 000 Stokes flow elements and prescribing nodal velocities along the solid–fluid interface to be zero. As the inner channel is half the width of the outer channels, the computed maximum velocity in the inner channel is twice that of the maximum velocity on the inlet and outlet boundaries. Figure 3 displays the velocity magnitude and pressure contour plots for the Darcy–Stokes flow model. The entire domain (fluid and solid material) shown in Figure 1 was discretized using a 200×100 element mesh and fluid velocities were prescribed to be zero on the exterior domain boundary with the exception of the inlet and outlet prescribed flows. The solid material permeability was set to $\kappa = 10^{-8}$. The velocity contour plots are nearly identical in shape and magnitude, demonstrating that the Darcy regularization achieves correct velocities for void elements and near-zero velocities at solid elements.

The performance of the Darcy–Stokes model is further examined by solving the channel flow problem using different magnitudes for the solid phase permeability. Table I contains these results. Note that the maximum nodal fluid velocity of a solid element decreases approximately linearly with the material permeability until about $\kappa = 10^{-10}$, where the computed maximum

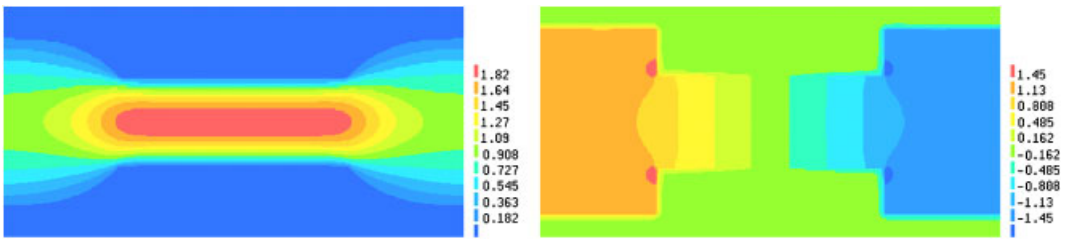

Figure 3. The velocity magnitude (left) and pressure (right) contours for the channel flow problem obtained using Darcy–Stokes finite elements with material permeability $k = 10^{-8}$. The maximum computed velocity is 2.00 occurring in the narrow channel.

Table I. Numerical results for the no-slip convergence study of the channel topology.

Finite element model	Material permeability κ	Max velocity of fluid	Max nodal velocity of solid element
Stokes flow, no-slip boundary conditions	—	2.00	0
Darcy–Stokes	10^{-4}	2.00	5.85 (10^{-3})
Darcy–Stokes	10^{-6}	2.00	6.01 (10^{-5})
Darcy–Stokes	10^{-8}	2.00	6.02 (10^{-7})
Darcy–Stokes	10^{-10}	1.97	6.29 (10^{-9})
Darcy–Stokes	10^{-12}	1.51	6.02 (10^{-10})

narrow channel velocity reveals that the model begins to lose accuracy. It is important to note that the results shown in Table I are for the 200×100 element mesh. We have found that more course meshes lose accuracy at higher values of permeability. Results for this and other test cases suggest this loss of accuracy begins when the relationship between permeability and maximum nodal velocity in a solid element becomes noticeably non-linear. Therefore, when implementing the Darcy regularization for impermeable solid material, some care must be taken in determining the minimum allowable material permeability $\kappa_{\min}$. This issue is discussed further in Section 4. It should also be noted that using small values of permeability can lead to poorly conditioned systems of equations as the viscosity stiffness matrices of solid elements become proportionately large.

3.4. Eliminating intermediate volume fractions

In approximating the adherence condition the Darcy–Stokes formulation will also prevent intermediate volume fractions from appearing in the final solution. For low-permeability material, the Darcy component will dominate the element stiffness computation and greatly reduce the corresponding nodal velocities. The only way to eliminate the Darcy component is for the element to be a true void ($\rho^e = 0$). As the volume of voids is limited, intermediate volume fractions become 'uneconomical'. This approach has similarities to the solid isotropic material with penalization method (SIMP) for steering minimum compliance solutions towards a 0–1 distribution [14]. The SIMP method sets element stiffness tensors proportional to $(\rho^e)^\eta$, where generally $\eta \geqslant 3$, thereby decreasing the stiffness of elements with volume fractions less than 1.

Minimum compliance is a maximum stiffness problem and so SIMP reduces the stiffness of elements with intermediate volume fractions. Maximizing fluid flow is a minimum stiffness problem and so we have increased the stiffness of elements with intermediate volume fractions.

The results presented in Section 5 demonstrate that this technique is successful in producing 0–1 topologies. Solutions are completely free of elements with intermediate volume fractions—regions of artificial material, or so-called grey regions, cannot be found in any of the solutions. Solutions presented in Reference [15], however, do contain grey regions, particularly along the solid–fluid interface. This tends to blur the boundary between the fluid and solid regions.

An alternative penalization of intermediate densities is to artificially raise the stiffness of such elements via an exponent. The Darcy and Stokes stiffness matrices could be combined, for example, in the following manner:

$$\mathbf{k}^e_{\mathrm{ds}}(\rho^e) = (1-\rho^e)^{1/\eta}\mathbf{k}^e_{\mathrm{s}} + (\rho^e)^{1/\eta}\mathbf{k}^e_{\mathrm{d}} \tag{21}$$

where $\eta > 1$. The coefficients of the Darcy and Stokes stiffness matrices are thus artificially raised for elements with intermediate volume fractions, making them uneconomical. In a sense this is an inverse version of the SIMP method and would be useful when the material phase has a relatively high permeability. This implementation was not necessary for this work.

4. SOLVING THE OPTIMIZATION PROBLEM

The relaxed design optimization problem with Darcy regularization is now stated as

$$\begin{aligned} &\min_{\rho^e} \ \Phi(\rho^e) \\ &\text{subject to:} \quad \sum_{e\in\Omega}(1-\rho^e)v^e \leqslant V_{\mathrm{f}} \\ &\qquad\qquad 0 \leqslant \rho^e \leqslant 1 \quad \forall e \in \Omega \end{aligned} \tag{22}$$

where $\Phi(\rho^e)$ is the minimum total potential power subject to the divergence condition as given by Equation (11).

This problem can be interpreted as minimizing the rate at which energy is dissipated in the fluid while maximizing the fluid velocities at locations of nodal forces. As we will neglect body forces, problem (22) is referred to as a minimum dissipated power problem.

4.1. Avoiding local minima

Local minima, in general, can be avoided with an intelligent initial guess. However, we will not rely upon this and all examples will be solved with a uniform initial distribution of material. In order to reduce the probability of converging to a local and not global minimum, a continuation method will be used. The material permeability κ used in the Darcy regularization controls the degree of penalization on nodal velocities of solid elements and elements with intermediate volume fractions. If this penalty is too great at the outset, the algorithm is likely to converge to a local minimum. This characteristic was also reported by Borrvall and Petersson [15] and is a well-documented difficulty in structural optimization. Therefore, the optimization problem

is first solved with a relatively high permeability, and κ is decreased in subsequent iterations. This pattern continues until (i) $\kappa<\kappa_{\max}$ and intermediate volume fractions have been sufficiently reduced or (ii) $\kappa=\kappa_{\min}$. The parameter $\kappa_{\max}$ is selected as the maximum permeability where the adherence condition is adequately enforced. The parameter $\kappa_{\min}$ is selected to be a small positive number that insures numerical stability. As previously mentioned, the maximum nodal velocity of a solid element decreases nearly linearly with permeability when the model is stable. Therefore, when permeability is decreased the flow problem should be solved for the current topology. If a proportional drop is not seen in the maximum nodal velocity of solid elements, the permeability is returned to its previous magnitude and assigned to $\kappa_{\min}$ (or a smaller decrease should be tested). This will also insure stability of the optimization algorithm. The power dissipated in an element e is defined as $\tilde{\mathbf{u}}^{e^{\mathrm{T}}}\mathbf{k}_{\mathrm{ds}}^{e}\tilde{\mathbf{u}}^{e}$, where $\tilde{\mathbf{u}}^{e}$ is the complete velocity vector (unknown and prescribed) for element e. Therefore, if permeability is decreased below $\kappa_{\min}$, the Darcy viscosity stiffness matrix will increase without a corresponding drop in velocities, causing the computed power dissipated in the element to increase. Note that if a permeable matrix material is used, κ is reduced to the actual permeability of the material.

The continuation method described above is not sufficient to prevent convergence to local minima. Solutions can be overly influenced by topologies generated at early stages of the continuation method where permeability is relatively high. This can lead to the development of 'humps' along the boundaries of solid regions that are known to increase power dissipation [27]. Borrvall and Petersson also reported convergence to local minima for some design problems and implemented a two-step design process using different parameter values when such instances occurred. We avoid local minima by smoothing solutions at early stages of the design. Rather than apply a heuristic filter, we implement a technique developed by Guest *et al.* [28] for imposing a minimum length scale in topology optimization. The technique introduces nodal volume fractions, denoted as ρ_n, as the design variables instead of element volume fractions. These nodal values are then projected onto element space via a regularized Heaviside function to determine the elementwise ρ^e that define topology. Using nodal design variables tends to produce smoother topologies as a single design variable influences several element volume fractions. This inherent smoothing appears to move solutions off of local minima and yields better solutions. The technique is discussed briefly in Section 4.2.

It must be emphasized that we are implementing the nodal design variable approach to avoid local minima and *not* for the purpose of imposing a minimum length scale. The minimum dissipated power formulation for fluids as presented is well posed. This is unlike the minimum compliance problem for elasticity that is ill posed and causes (among other difficulties) a numerical instability known as mesh dependence, a feature where mesh refinement leads to the development of finer, more intricate topologies. Mesh dependence is not an issue in the minimum dissipated power problem, however, as more intricate topologies would increase the length (or area) of the fluid–solid interface, locations at which the velocities are zero. Therefore, assuming the mesh is sufficiently refined, solutions will be independent of the mesh size and it is not necessary to impose a minimum length scale on voids (or solids). This characteristic will be shown here and was reported in Reference [15].

4.2. Smoothing with nodal design variables

The nodal design variable method presented in Reference [28] was shown to be capable of imposing a minimum length scale and obtaining 0–1 topologies in structural optimization. We

will summarize the approach here, although the reader is referred to the original work for details.

Defining $r_{\min}$ as the minimum allowable radius of solid phase members in the final topology, all nodes within a distance $r_{\min}$ of the centroid of an element e influence the element's volume fraction ρ^e. This can be visualized by drawing a circular sub-domain Ω_w^e of radius $r_{\min}$ around the centroid of e as shown in Figure 4. Nodes located inside Ω_w^e contribute to the computation of ρ^e. These nodal volume fractions ρ_n are projected onto the element e via the following regularized Heaviside function:

$$\rho^e = 1 - \mathrm{e}^{-\beta\mu^e(\rho_n)} + \zeta^e(\rho_n) \tag{23}$$

where the parameter β dictates the curvature of the regularization, with $\beta = 0$ resulting in a linear regularization and $\beta = \infty$ approaching the Heaviside function. Generally, β is initially chosen to be small (e.g. $\beta = 5$) and is raised in subsequent iterations to allow convergence to a 0–1 topology. The function $\zeta^e(\rho_n)$ recovers the bounds on the element volume fractions and is given by

$$\zeta^e = \mu^e(\rho_n)\mathrm{e}^{-\beta} \tag{24}$$

The function $\mu^e(\rho_n)$ is the linear weighted average of the volume fractions of nodes located inside Ω_w^e, i.e.:

$$\mu^e = \frac{\sum_{j\in\Omega_w^e} \rho_j w(\mathbf{x}_j - \bar{\mathbf{x}}^e)}{\sum_{j\in\Omega_w^e} w(\mathbf{x}_j - \bar{\mathbf{x}}^e)} \tag{25}$$

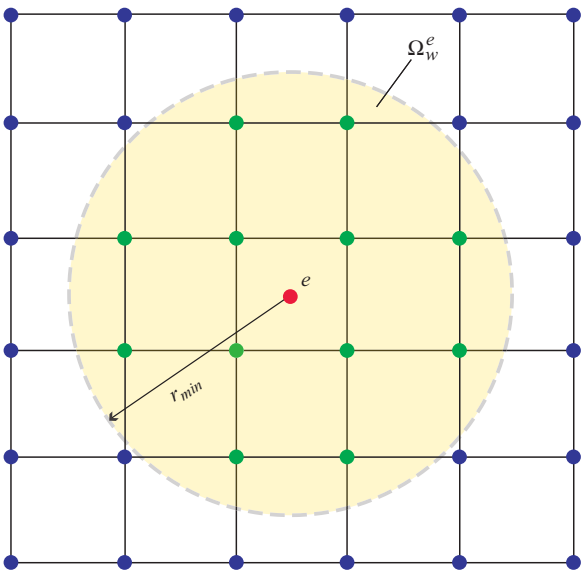

Figure 4. Nodes located inside the domain Ω_w^e are used in the projection scheme for element e.

where $\mathbf{x}_j$ is the location of node j and $\bar{\mathbf{x}}^e$ is the location of the centroid of element e. The magnitude of the weighting function w for a given node is based on the proximity of that node to the element centroid, with closest nodes receiving the greatest weight:

$$w(\mathbf{x}-\bar{\mathbf{x}}^e)=\begin{cases}\dfrac{r_{\min}-\|\mathbf{x}-\bar{\mathbf{x}}^e\|}{r_{\min}} & \text{if } \mathbf{x}\in\Omega_w^e\\ 0 & \text{otherwise}\end{cases} \tag{26}$$

Recall that we are employing this technique here for the purpose of avoiding local minima and *not* for imposing a minimum length scale. Therefore, the initial $r_{\min}$ will be decreased slowly over the optimization algorithm until it reaches the minimum value—i.e. until the projection function of an element contains only the nodes defining that element. This allows us to take advantage of the smoothing characteristic of the technique during the early design iterations without enforcing a minimum length scale criterion on the final design.

Implementing this technique requires only minor modifications to the original flow problem. The elementwise volume fractions ρ^e that define topology are simply expressed as a function of nodal volume fractions ρ_n. The objective function and volume constraint remain the same, while the design variable bounds are applied to the ρ_n and the optimization is performed with respect to ρ_n.

The minimum dissipated power problem with nodal design variables is written as

$$\begin{aligned}&\min_{\rho_n}\ \Phi(\rho_n)\\ &\text{subject to:}\quad \sum_{e\in\Omega}(1-\rho^e(\rho_n))v^e\leqslant V_{\mathrm{f}}\\ &\qquad\qquad 0\leqslant\rho_n\leqslant 1\quad \forall n\in\Omega\end{aligned} \tag{27}$$

4.3. Solution algorithm

Problem (27) is solved using fixed-point iterations. Velocities for the current iteration are found by solving the minimum potential power for the current set of element volume fractions. This corresponds to solving the Darcy–Stokes equilibrium equations (18).

The velocities are then held constant and the outer optimization problem is solved to determine the new volume fractions:

$$\begin{aligned}&\min_{\rho_n}\ \frac{1}{2}\sum_e \tilde{\mathbf{u}}^{e\mathrm{T}}\mathbf{k}_{\mathrm{ds}}^e(\rho^e(\rho_n))\tilde{\mathbf{u}}^e-\rho_{\mathrm{f}}(\mathbf{b}_{\mathrm{u}})^{\mathrm{T}}\mathbf{u}\\ &\text{subject to:}\quad \sum_{e\in\Omega}(1-\rho^e(\rho_n))v^e\leqslant V_{\mathrm{f}}\\ &\qquad\qquad 0\leqslant\rho_n\leqslant 1\quad \forall n\in\Omega\end{aligned} \tag{28}$$

where $\tilde{\mathbf{u}}^e$ is the complete velocity vector (unknown and prescribed) for element e and the total dissipated power has been expressed as a summation of elemental dissipated powers. It

is useful to note that objective function of (28) is equivalent to

$$\Phi(\rho_n) = \frac{1}{2} \sum_{e \in \Omega} (\mathbf{u}^{e^{\mathrm{T}}} \mathbf{k}_{\mathrm{ds}}^{e}(\rho^e(\rho_n))\mathbf{u}^e + \mathbf{g}^{e^{\mathrm{T}}} \mathbf{k}_{\mathrm{ds}}^{e}(\rho^e(\rho_n))\mathbf{g}^e) - \mathbf{f}_{\mathrm{ds}}(\rho^e(\rho_n))^{\mathrm{T}}\mathbf{u} \tag{29}$$

Equation (29) resembles the minimum compliance problem in elasticity and so the optimization problem (28) is solved using the method of moving asymptotes (MMA) developed by Svanberg [29, 30]. MMA minimizes sequential convex approximations of the original function and is known to be very efficient for structural optimization problems. The convex sub-problem is then solved using an interior-point method, an efficient method for convex problems; see References [31, 32] for details on implementing the interior-point method.

To summarize, the algorithm is given by

1. Initialize ρ_n with an educated guess or uniform or random distribution. Solve the equilibrium equation (18) with the initial κ to find the initial nodal velocities $\mathbf{u}$.
2. Create a convex approximation to problem (28) using MMA and solve for ρ_n using the interior-point algorithm.
3. Solve the equilibrium equation (18) for the new ρ_n to find the new nodal velocities $\mathbf{u}$.
4. If MMA has not converged, go to step 2.
   Else:
   Increase β, decrease $r_{\min}$.
   If ($\kappa > \kappa_{\max}$) or (significant intermediate ρ^e still exist and $\kappa > \kappa_{\min}$):
   decrease[§] κ, solve Equation (18) for $\mathbf{u}$, go to step 2.
   Else: end.

5. RESULTS

The example problems contained in this section were also solved by Borrvall and Petersson [15]. For all problems the solid phase is impermeable, body forces are neglected and, unless otherwise noted, non-zero prescribed flow profiles are normal to the boundary and computed by

$$\mathbf{g}(x) = g^* \left(1 - \left(\frac{2x}{l}\right)^2\right) \tag{30}$$

where g^* is the prescribed velocity at the centre of the flow profile, l is the length of the flow profile, and x is location within the flow profile ($x \in [-l/2, l/2]$). Although not stated in Reference [15], pressure is prescribed to be zero at the centre of the design domains to improve performance of iterative solvers. All problems were solved using 4-node quadrilateral elements, unit viscosity, and a uniform initial distribution of material.

For convenience, initial permeability κ will be expressed in terms of a mesh-specific reference permeability κ_h, chosen to be the permeability at which the diagonal terms of the Stokes and Darcy viscosity stiffness matrices are equal. For 4-node square elements, κ_h is computed as $\kappa_h = 0.0\bar{5}h^2$ where h is the element size.

[§]Note that κ should not be decreased below the actual permeability of the solid material when designing with permeable matrix material.

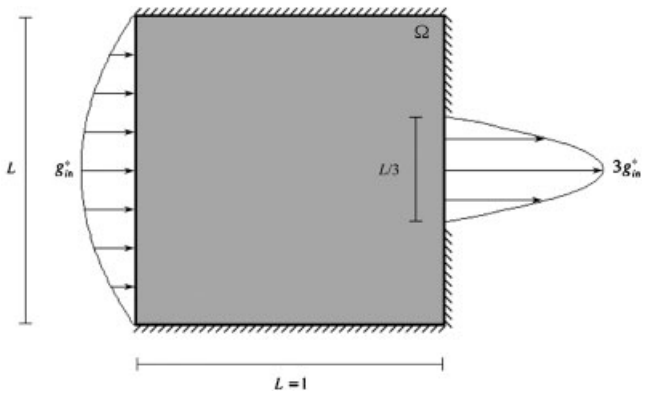

Figure 5. The diffuser design problem.

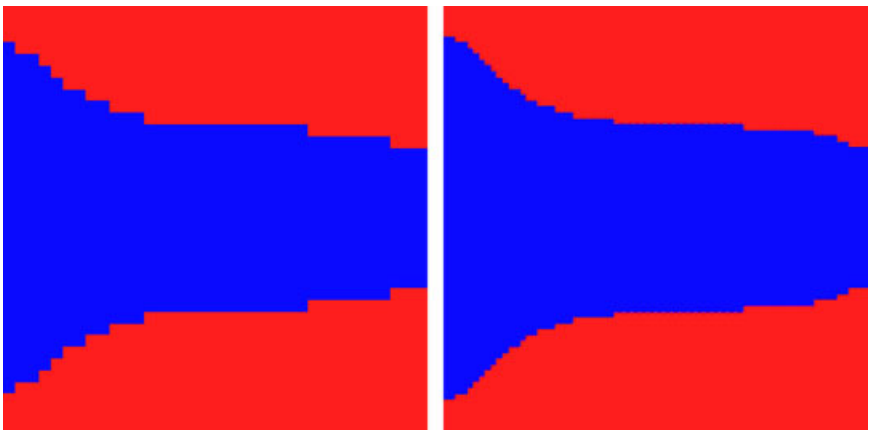

Figure 6. Solution to the diffuser problem using 36×36 (left) and 72×72 (right) element meshes.

5.1. Diffuser example

A diffuser problem is shown in Figure 5 and treated here as dimensionless. The design domain Ω is square with a side length L of 1. The maximum inlet velocity g^*_{in} is 1 and the maximum outlet velocity is 3. The inlet and outlet flows are shown in the figure and velocity is prescribed to be zero elsewhere on the boundary of the domain. Initial permeability is $10\kappa_h$, $r_{\min}$ is initially 0.06 units, and the allowable volume V_{f} of the fluid is 50% of the domain volume.

The diffuser problem was solved using several size meshes, two of which are shown in Figure 6. The solution is independent of the mesh discretization: the only difference between the topologies is that the boundary of the structure becomes smoother with mesh refinement.

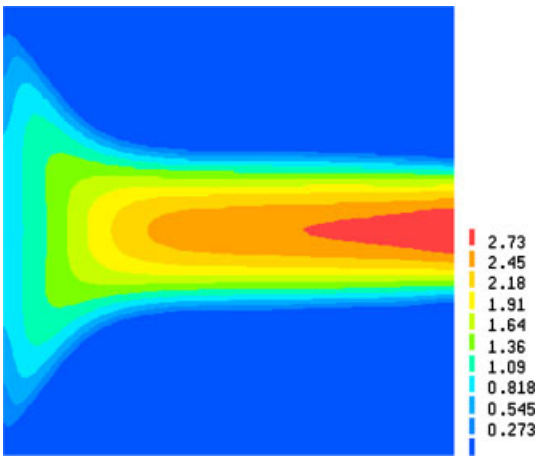

Figure 7. Velocity magnitude contour plot demonstrating simulation of the no-slip condition for the diffuser topology shown in Figure 6. Plot was created using a 102×102 Darcy–Stokes element mesh with $k = 10^{-8}$.

These solutions are nearly identical to those presented in Reference [15], the primary difference being that those solutions contain a small portion of intermediate volume fractions. The topologies shown in Figure 6 are clear solid–void solutions—there are no regions of fictitious material.

A contour plot of velocities for the final solution is shown in Figure 7 and was created using a 102×102 mesh of Darcy–Stokes elements with $\kappa = 10^{-8}$. All velocity magnitudes in solid elements and on the solid–fluid interface are less than 10^{-8}, demonstrating that the adherence condition has been achieved with the Darcy regularization.

5.2. Minimum drag topology example

A minimum drag problem is shown in Figure 8 and treated here as dimensionless. The design domain Ω is square with a side length L of 1. The fluid velocity is prescribed everywhere on the boundary to be of unit magnitude (g^*) in the horizontal direction. The exterior of the design domain is assumed (and held) to be fluid as shown by Figure 8. Initial permeability is $\kappa = 100\kappa_h$, $r_{\min}$ is initially 0.06 units, and several values of the allowable volume of fluid V_f are examined.

Similar problems have been studied in the context of shape optimization of rigid bodies: theoretically by Pironneau [4, 5] and numerically by (for example) Glowinski and Pironneau [27] and Kim and Kim [6]. More recently, Lund *et al.* [7] applied shape optimization to minimize drag on a flexible body. Of particular interest to the example problem given here, the rigid-body works suggest that the front wedge of the solid material should be at an angle of 90°.

This feature is observed reasonably well in the solutions shown in Figure 9 as the designs are able to maintain the same shape for the front wedge despite varying quantities of allowable fluid volume. The topologies presented in Reference [15] appear to be smoother versions of

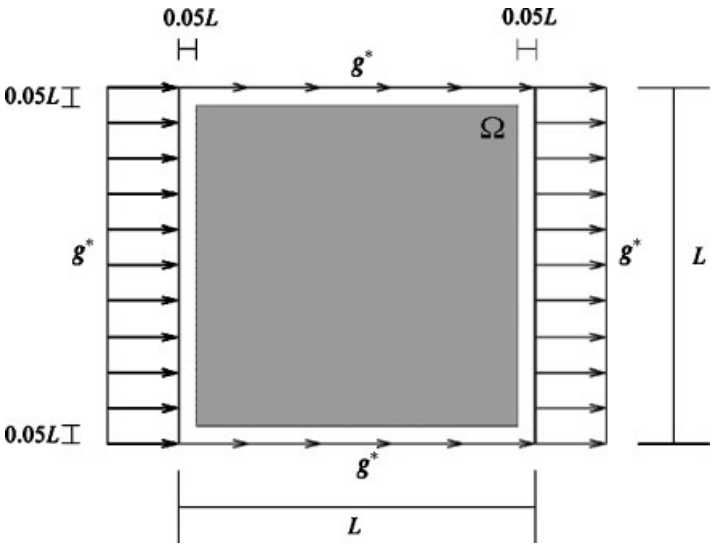

Figure 8. The minimum drag design problem.

topologies shown in Figure 9. However, this effect is due to the presence of intermediate volume fractions that blur the boundary of the solid material.

A contour plot of velocities for the minimum drag topology of Figure 9(b) is shown in Figure 10. All velocity magnitudes in solid elements and on the solid–fluid interface are less than 10^{-8}, again demonstrating that the adherence condition has been achieved with the Darcy regularization. The contour plot was created using a 100×100 element mesh with $\kappa = 10^{-8}$.

5.3. Double pipe example

A double pipe problem is shown in Figure 11 and treated here as dimensionless. The design domain Ω has a length of L (to be specified) and unit height H. The domain has two inlet and outlet flows, each with a unit maximum velocity g^*, and velocity is prescribed to be zero elsewhere on the boundary of the domain. Initial permeability is $\kappa = 10\kappa_h$, $r_{\min}$ is initially 0.05, and the allowable volume V_f of the fluid is one-third of the domain volume.

The simplest solution to this problem is to have two single straight pipes connecting the inflows to the outflows. This is the optimal solution for L/H ratio of 1. For longer flow distances (e.g. $L/H = 1.5$), however, the two pipes join to form a single, wider pipe through the centre of the domain as Figure 12 illustrates. This design decreases the length of the fluid–solid interface, thereby decreasing the power lost. Although the topologies agree with those presented here, the solutions in Borrvall and Petersson [15] contain regions of artificial material and do not sufficiently account for the adherence condition. It is stated in Reference [15] that numerical results include power dissipated in the solid regions which means velocities have not been adequately reduced along the solid–fluid interface to accurately model flow through the pipes.

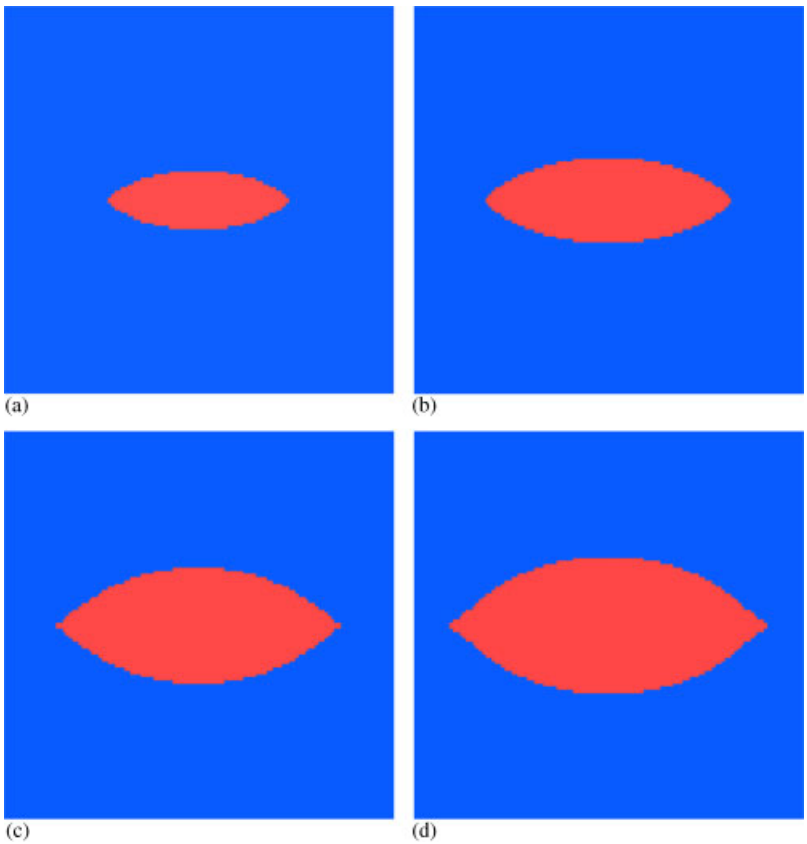

Figure 9. The minimum drag topology for various required volumes of solid material: (a) 5%; (b) 10%; (c) 15%; and (d) 20% of the total domain volume. Note that the front wedge is a similar shape for all topologies. Topologies were created using a 120×120 element mesh.

6. CONCLUSIONS

This paper presents a new methodology for the topology optimization of creeping fluid flows. Operating in a two-phase solid–void domain, the goal is to minimize the dissipated power in the fluid by determining the optimal distribution of voids through which the fluid flows. The binary constraint on the design variable ρ^e is regularized by treating the solid phase as a porous medium. Consequently, the field equations are constructed so that flow through voids is governed by Stokes flow while flow through solid material is governed by Darcy's law. When the solid phase is impermeable, the discrete no-slip condition is simulated by assigning a low permeability to the solid phase.

The work of Borrvall and Petersson [15] was the first to use topology optimization to design continuum domains for fluid transport. The no-slip condition is regularized in Reference [15] via a numerical damping term that is large for solid elements to slow velocities and near zero for void elements so that Stokes equations dominate. The damping term is derived from a

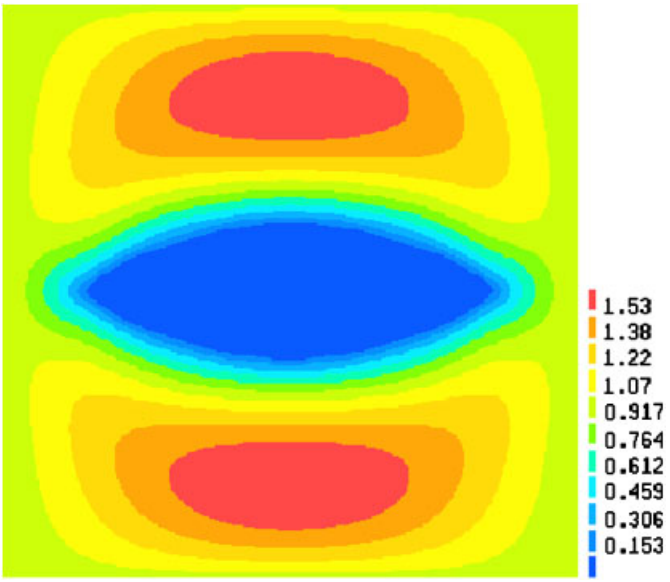

Figure 10. Velocity magnitude contour plot demonstrating simulation of the no-slip condition for the minimum drag topology shown in Figure 9(b). Plot was created using a 100×100 Darcy-Stokes element mesh with $k = 10^{-8}$.

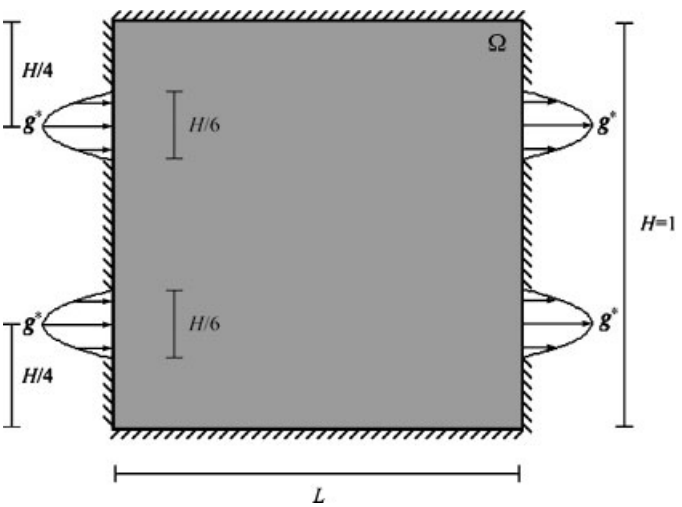

Figure 11. The double pipe design problem.

Coulette flow assumption and, as presented, the technique is limited to approximating the no-slip condition—i.e. is limited to optimizing the layout of an impermeable solid material. On the other hand, the Darcy regularization presented here is shown to effectively simulate the no-slip

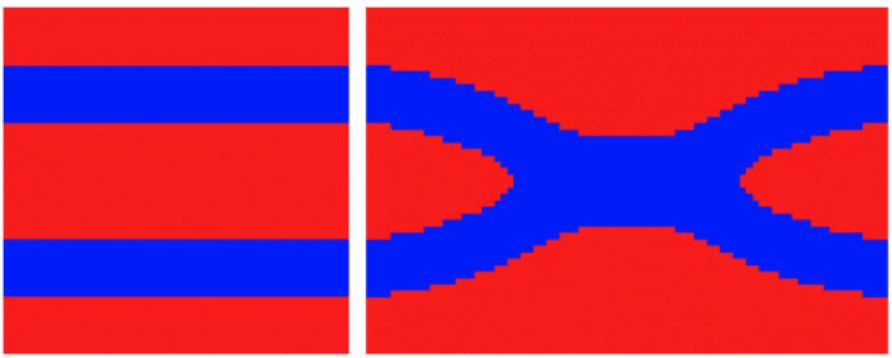

Figure 12. Solution to the double pipe design problem for $L/H = 1.0$ (left) and $L/H = 1.5$ (right). As the length to height ratio of the domain increases, the two pipes join to form a single, wider pipe. Topology at right was created using a 54×81 element mesh.

condition and, as we believe will be shown by future work, can be used to optimize the layout of a permeable solid material. Such would be the objective in the design of (for example) slow flow filters where the Darcy and Stokes equations are the governing equations in the solid and fluid phase, respectively. This potentially opens a new class of problems to which this technique applies. Note, however, that the objective function would have to be reformulated to correctly account for power dissipated in fluid flowing through the porous medium. Additionally, while both methodologies produce similar overall topologies, the solutions presented here are 0–1 topologies and do not contain elements with intermediate volume fractions. This is in contrast to solutions presented in Reference [15] that contain regions of artificial material.

A significant advantage of the presented Darcy–Stokes approach is that the coupled flow problem is solved using existing stabilized mixed finite element methods with velocity and pressure variables. The Babuska–Brezzi condition for the Stokes and Darcy equations is circumvented by using the stabilizations of Hughes *et al.* [18] and Masud and Hughes [19], respectively. These techniques allow equal-order interpolations for both the velocity and pressure fields. We have found this approach to be sufficient for modelling the coupled flow and simulating the no-slip condition, and have not implemented special boundary conditions, auxiliary meshes, or additional stabilization techniques along the solid–fluid interface. This is in contrast to the approach in Reference [15] where different size meshes are used to solve the pressure and velocity fields. The only limitation is that some care must be taken in selecting the minimum allowable material permeability below which numerical instability seems to occur. This parameter, however, is easily determined using the continuation method discussed in Section 4.1. The actual convergence properties of the Darcy–Stokes equations to the no-slip condition are the subject of future work.

The topology optimization methodology presented here is capable of designing devices for transport of creeping flows of viscous fluids. While the stated objectives included minimizing dissipated power and minimizing drag, the method is also applicable to the design of valves for minimum head loss and ideally would be extended to handle design problems not limited to a single set of boundary conditions [15]. Further, we have used the methodology and Darcy regularization to design periodic porous materials with maximized permeability [33, 34]. Assuming flow through the channels of the microstructure is governed by Stokes equations

and that the matrix material is impermeable so that the no-slip condition holds, an inverse homogenization problem is formulated and solved in these works to maximize the effective permeability of the bulk material. The optimal topology appears to be a minimal surface, plausible as this minimizes the fluid–structure interface where velocities are zero. When used together, the inverse homogenization technique and the methodologies presented here offer the potential for designing on two length scales. That is, optimizing the macroscopic layout of a permeable material as well as the porous microstructure of that material, an idea that has been voiced as a future objective of structural optimization.

ACKNOWLEDGEMENTS

This work is supported by the NASA University Research, Engineering and Technology Institute on Bio Inspired Materials (BIMat) under award No. NCC-1-02037. This support is gratefully acknowledged.

REFERENCES

1. Sritharan SS (ed.). *Optimal Control of Viscous Flow*. SIAM: Berlin, 1998.
2. Ghattas O, Bark J-H. Optimal control of two- and three-dimensional incompressible Navier–Stokes flows. *Journal of Computational Physics* 1997; **136**:231–244.
3. Collis SS, Ghayour K, Heinkenschloss M, Ulbrich M, Ulbrich S. Optimal control of unsteady compressible viscous flows. *International Journal for Numerical Methods in Fluids* 2002; **40**:1401–1429.
4. Pironneau O. On optimum profiles in Stokes flow. *Journal of Fluid Mechanics* 1973; **59**:117–128.
5. Pironneau O. On optimum design in fluid mechanics. *Journal of Fluid Mechanics* 1974; **64**:97–110.
6. Kim DW, Kim M-U. Minimum drag shape in two-dimensional viscous flow. *International Journal for Numerical Methods in Fluids* 1995; **21**:93–111.
7. Lund E, Møller H, Jakobsen LA. Shape design optimization of stationary fluid–structure interaction problems with large displacements and turbulence. *Structural and Multidisciplinary Optimization* 2003; **25**:383–392.
8. Cabuk H, Modi V. Optimum plane diffusers in laminar flow. *Journal of Fluid Mechanics* 1992; **237**:373–393.
9. Madsen JI, Olhoff N, Condra TJ. Optimization of straight, two-dimensional diffusers by wall contouring and guide vane insertion. *Proceedings of World Congress of Structural and Multidisciplinary Optimization*, vol. 3, Buffalo, NY, 1999; 43-EOA3-3.
10. Lund E, Møller H, Jakobsen LA. Shape optimization of fluid–structure interaction problems using two-equation turbulence models. *AIAA Proceedings of the 43rd AIAA/ASME/ASCE/AHS/ASC Structures*, *Structural Dynamics*, *and Materials Conference and Exhibit*, Denver, CO, 2002, *AIAA Paper 2002-1478*.
11. Borggaard J, Burns J. A PDE sensitivity equation method for optimal aerodynamic design. *Journal of Computational Physics* 1997; **136**:366–384.
12. Cliff EM, Heinkenschloss M, Shenoy A. Airfoil design by an all-at-once method. *International Journal for Computational Fluid Mechanics* 1998; **11**:3–25.
13. Bendsøe MP, Sigmund O. *Topology Optimization*: *Theory*, *Methods and Applications*. Springer: Berlin, 2003.
14. Bendsøe MP. Optimal shape design as a material distribution problem. *Structural Optimization* 1989; **1**:193–202.
15. Borrvall T, Petersson J. Topology optimization of fluids in Stokes flow. *International Journal for Numerical Methods in Fluids* 2003; **41**:77–107.
16. Babuska I. Error bounds for finite element method. *Numerische Mathematik* 1971; **16**:322–333.
17. Brezzi F. On the existence, uniqueness and approximation of saddle-point problems arising from Lagrange multipliers. *Revue Francaise d'Automatique Informatique Recherche Operationnelle* 1974; **8, R-2**:129–151.
18. Hughes TJR, Franca LP, Balestra M. A new finite element formulation for computational fluid dynamics: V. Circumventing the Babuska–Brezzi condition: a stable Petrov–Galerkin formulation of the Stokes problem accommodating equal-order interpolations. *Computer Methods in Applied Mechanics and Engineering* 1986; **59**:85–99.

19. Masud A, Hughes TJR. A stabilized mixed finite element method for Darcy flow. *Computer Methods in Applied Mechanics and Engineering* 2002; **191**:4341–4370.
20. Layton WJ, Schieweck F, Yotov I. Coupling fluid flow with porous media flow. *SIAM Journal on Numerical Analysis* 2003; **40**:2195–2218.
21. Burman E, Hansbo P. A unified stabilized method for Stokes' and Darcy's equations. Chalmers Finite Element Center, Chalmers University of Technology, Göteborg, Sweden.
22. Shavit U, Bar-Yosef G, Rosenzweig R, Assouline S. Modified Brinkman equation for a free flow problem at the interface of porous surfaces: the Cantor–Taylor brush configuration case. *Water Resources Research* 2002; **38**(12):1320–1334.
23. Kim S, Russel WB. Modelling of porous media by renormalization of the Stokes equations. *Journal of Fluid Mechanics* 1985; **154**:269–286.
24. Beavers GS, Joseph DD. Boundary conditions at a naturally permeable wall. *Journal of Fluid Mechanics* 1967; **30**:197–207.
25. Saffman PG. On the boundary condition at the surface of a porous medium. *Studies in Applied Mathematics* 1971; **50**:93–101.
26. Nassehi V, Hanspal NS, Waghode AN, Ruziwa WR, Wakeman RJ. Finite-element modeling of combined free/porous flow regimes: simulation of flow through pleated cartridge filters. *Chemical Engineering Science* 2005; **60**:995–1006.
27. Glowinski R, Pironneau O. On the numerical computation of the minimum-drag profile in laminar flow. *Journal of Fluid Mechanics* 1975; **72**:385–389.
28. Guest JK, Prévost JH, Belytschko T. Achieving minimum length scale in topology optimization using nodal design variables and projection functions. *International Journal for Numerical Methods in Engineering* 2004; **61**:238–254.
29. Svanberg K. The method of moving asymptotes—a new method for structural optimization. *International Journal for Numerical Methods in Engineering* 1987; **24**:359–373.
30. Svanberg K. A globally convergent version of MMA without linesearch. In *Proceedings of the First World Congress of Structural and Multidisciplinary Optimization*, Goslar, Germany, Rozvany GIN, Olhoff N (eds), 1995; 9–16.
31. Vanderbei RJ, Shanno DF. An interior-point algorithm for nonconvex nonlinear programming. *Computational Optimization and Applications* 1999; **13**:231–252.
32. Benson HY, Shanno DF, Vanderbei RJ. Interior-point methods for nonconvex nonlinear programming: filter methods and merit functions. *Computational Optimization and Applications* 2002; **23**:257–272.
33. Guest JK. Design of optimal porous material structures for maximized stiffness and permeability using topology optimization and finite element methods. *Ph.D. Thesis*, Department of Civil and Environmental Engineering, Princeton University, 2005.
34. Guest JK, Prévost JH. Design of maximum permeability material structures. *Computer Methods in Applied Mechanics and Engineering*, under review.

